Journal of Civil Engineering and Materials Application
Journal home page: http://jcema.com

Received: 01 October 2023 • Revised: 05 November 2023 • Accepted: 01 December 2023

Research

doi: 10.22034/jcema.2024.432780.1128

Investigating the Effects of Increasing the Span Length to the Story Height of the Bracing Frame under Near-Fault and Far-Fault Earthquakes

Masoud Mahdavi [2]*, Abbas Babaafjaei [2], SeyyedReza Hosseini [2], Bamdad Aghababaei Mornani [2], Mohsen Tavakoli [2]

[1] Ph.D. Student, Faculty of Civil Engineering, K. N. Toosi University of Technology, Tehran, Iran.
[2] M.Sc. Student, Faculty of Civil Engineering, K. N. Toosi University of Technology, Tehran, Iran.

*Correspondence should be addressed to Masoud Mahdavi, Ph.D. Student, Faculty of Civil Engineering, K. N. Toosi University of Technology, Tehran, Iran Tel:+ 09052180420; Email: dr.civil.book@gmail.com

ABSTRACT

The passive control of the structure with bracing system is one of the new methods of structural engineering. Indicators such as the span length and the story height have important effects on the steel structure performance during an earthquake. Determining the relationship between various geometric indicators and the seismic performance of structure leads to better design and reduction of damages during an earthquake. In the current research, a 5-story steel frame with Gate brace was designed with Sap2000 software. The K index was defined as the ratio of the span length to the story height. Three different values of K equal to 1, 2 and 3 were defined in the modelling of the structure. The structures were analyzed by the modal time history analysis method under the accelerometers of Kobe (near-fault) and El Centro (far-fault). The results showed that in the near-fault area, Modal damping energy and base shear force have a direct relationship with the K index. The mentioned 2 seismic parameters, in the far-fault area, do not have a clear relationship with the K index. Also, parameters such as acceleration, roof displacement, brace axial force, story displacement, column shear force and the support reaction force do not have a clear relationship with the K index in the near-fault and far-fault areas.

Keywords: Gate Brace; Near-Fault; Far-Fault; Modal Time History Analysis; Seismic Parameters

1. INTRODUCTION

Earthquakes can cause various types of damage to structures, including residential buildings, infrastructure, and other constructions [1–3]. The effects of earthquake on structures can be categorized into several types:

- Ground Shaking: The primary cause of earthquake damage to man-made structures is ground shaking, which can lead to structural damage and collapse, resulting in injury or death to occupants. The intensity of an earthquake is usually measured using the Richter scale [2,4,5].

- Landslides: Earthquakes can trigger landslides, which can cause catastrophic damage to homes and towns. He violent shaking of the ground produces the greatest property losses and personal injuries [6].

- Surface Faulting: The vibrations from an earthquake can lead to ground displacement and

surface rupture, causing damage to roads and buildings [2].

- Fire: Earthquakes can cause fires due to ruptured gas lines or other infrastructure, leading to additional damage and loss of life [7,8].

- Building Collapse: Earthquakes can cause buildings to collapse due to loss of bearing strength, which occurs when the soil supporting a building liquefies and loses strength, allowing the structure to settle and tip [9–11]. To minimize the effects of earthquakes on structures, engineers and architects use seismic load analysis methods that determine the strength and stability of buildings and other constructions. These methods help ensure the safety of residential structures during an earthquake. However, even with these measures in place, earthquakes can still cause significant damage [12,13].

Control systems in structures refer to the use of various techniques and devices to reduce vibrations, energy consumption, and improve the overall performance of the structure [14]. Structural control systems can be classified into two main categories:

- Passive Control Systems: These systems do not require external power or feedback to operate. They rely on the inherent properties of the structure or additional devices to dissipate or counteract the vibration energy. Examples of passive systems include base isolation, tuned mass dampers, and viscous dampers [15,16].

- Active Control Systems: These systems require external power and feedback to adjust their parameters or apply forces to the structure. They can actively monitor and control the structure's response to vibrations [17–19].

Lian et al. [20] investigated the effect of strain rate on the failure parameters of concrete beams with small span to height ratio. The results showed that the effect of the opening to height ratio on the performance of the member is high. Takadate and Uematsu [21] investigated the vibration mechanism of long-span flat roofs with different span-to-height ratios. Li et al. [22] conducted an experimental analysis and simulation of a shell structure with a large opening. They consider the impact of the span length on the performance level as effective and certain. Meng et al. [23] evaluated the collapse resistance of steel frame structures with different spans using finite element models. The results showed that increasing the opening dimensions and decreasing the resistance have a significant relationship. Tuan Pham et al. [24] investigated the load path mechanisms in beams with asymmetric span length. They considered the span to height ratio to be effective on seismic performance. Embaby et al. [25] determined the ultimate capacity of steel structures with large spans. The results showed that the presence of the large spans in the structure creates a different performance. Yu and Fang [26] investigated the structural damage model for the elastoplastic design of large-span structures. Gao et al. [27] investigated the performance of multi-span beams with graded graphene reinforced foams. The results showed that the taper ratio and the configuration of multi-span beams lead to large changes in the critical buckling load. Ci et al. [28] investigated the effect of axial load and span ratio on the seismic behavior of prefabricated structures for RC boundary elements. This research is an important reference for building design regulations. Artar and Carbas [29] designed the optimal size of steel frame structures under seismic excitations. Modeling was done with Sap2000 and Matlab software. The results were obtained by presenting the algorithm. Kalilzadeh Vahidi and Chavoshani [30] investigated the effect of increasing the span length and floor height on the progressive failure of reinforced concrete frames. The research was done with Opensees software and nonlinear static analysis method. The results showed that frames with 10%, 20% and 30% openings in the structure, their resistance decreased by 23, 31 and 39%. Zheng and Bay [31] investigated the effects of impact loads on the mechanical performance of the truss structure. In this research, different ratios of span length to height were investigated. The results showed a direct relationship between the span length and the stress. Wang et al. [32] investigated the effect of span length to height ratio of reinforced concrete slabs under blast loading. The results show the impact of the investigated index on the structural failure. Hasemi Razavi et al. [33] investigated the effect of span length on the progressive collapse behavior of steel anchor-resistant frames. They used several nonlinear static and dynamic analyzes to analyze three frames in the high seismic zone with different span lengths. The results showed that the beams and columns (in different span length to height ratios) have sufficient strength to withstand the drop of the column on the first story.

2. METHODOLOGY

2.1. Near and Far-Fault Earthquakes

Near and far-fault ground motions refer to the seismic waves generated by an earthquake in relation to a specific location. Near-fault ground motions occur close to the fault rupture, while far-fault ground motions occur at a significant distance from the fault rupture. Research has shown that near-fault ground motions possess significantly long-period pulses in the acceleration time history, which are consistent with velocity and displacement histories. The long-period response of near-fault ground motions is more excessive than that of far-fault ground motions. Studies have also demonstrated that near-fault ground motions can cause extensive damage to structures, and they are characterized by long-duration acceleration and pulse-like features in their velocity time history. Additionally, near-fault ground motions have been found to result in larger response values for structures compared to far-fault ground motions. Therefore, understanding the characteristics and effects of near-fault and far-fault ground motions is crucial for assessing the seismic hazard and designing earthquake-resistant structures [34–39].

Near-fault ground motions possess several unique characteristics that set them apart from far-fault ground motions. These characteristics include:

- Long-period pulses: Near-fault ground motions often contain strong coherent dynamic long-period pulses in their acceleration time history, which are consistent with velocity and displacement histories [40].
- These long-period responses are more excessive than those of far-fault ground motions. High-frequency content: Near-fault ground motions have a higher frequency content in their velocity time history, which contributes to their distinctive seismic wave characteristics [41].
- Forward-directivity: Near-fault ground motions exhibit forward-directivity, which means that the motion is more pronounced in the direction of the fault. Fling-step, hanging-wall, and significant [41].
- Vertical ground motion: Near-fault ground motions can be characterized by fling-step, hanging-wall, and significant vertical ground motion, which are not commonly observed in far-fault ground motions. Permanent ground displacement: Near-fault ground motions often involve permanent ground displacement, which is not typically observed in far-fault ground motions [41–43].
- Damage potential: Due to their long-duration acceleration and pulse-like features in their velocity time history, near-fault ground motions can cause extensive damage to structures [41].

Understanding these characteristics of near-fault ground motions is crucial for assessing seismic hazards and designing earthquake-resistant structures [2,41].

Far-fault ground motions, also known as far-field ground motions, have the following characteristics:

- Low Destructiveness: Far-field earthquakes are generally less destructive than near-field motions due to their low peak ground acceleration, peak ground velocity, and Arias intensity [44,45].
- Distinctive Features of Near-Fault Earthquakes: Near-fault earthquakes may contain distinct forward directivity pulse and fling step motion, which are not typically present in far-fault ground motions [44,45].
- Seismic Parameters: Far-fault ground motions differ from near-fault ground motions in terms of seismic parameters such as long-period velocity or displacement pulse-like records, which are typically very intense [44,45].

In summary, far-fault ground motions are characterized by their lower destructiveness compared to near-fault motions and the absence of distinctive features such as forward directivity and fling effect. Seismic parameters also differ between far-fault and near-fault ground motions, with far-fault motions exhibiting specific intense characteristics [41–46]. Figure (1) shows the characteristics of near and far-fault acceleration.

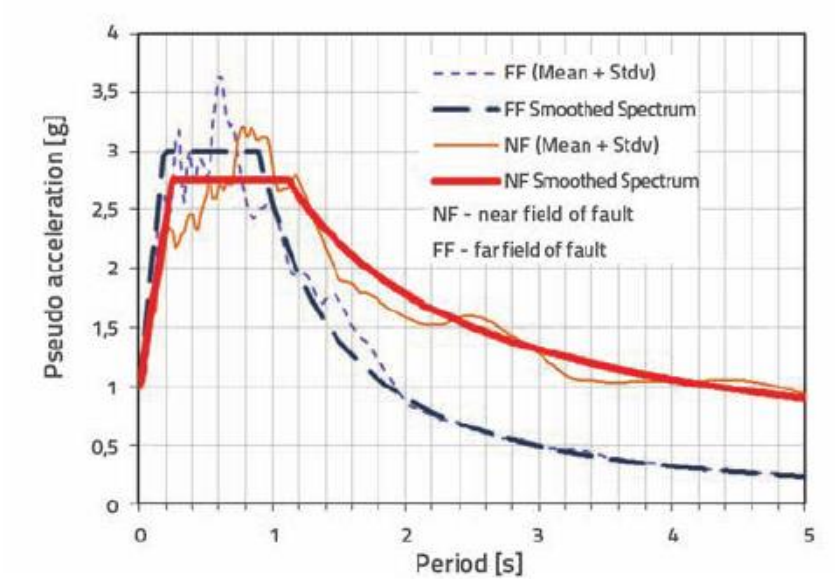

Figure 1. Characteristics of near and far-fault ground motions [47].

In this research, a 5-story steel frame with 3 spans is modelled in Sap2000 [48]. Gate bracing systems have been modelled and analyzed with the modal linear dynamic method. Figure (2) shows the designed models of gate bracing system in the current research.

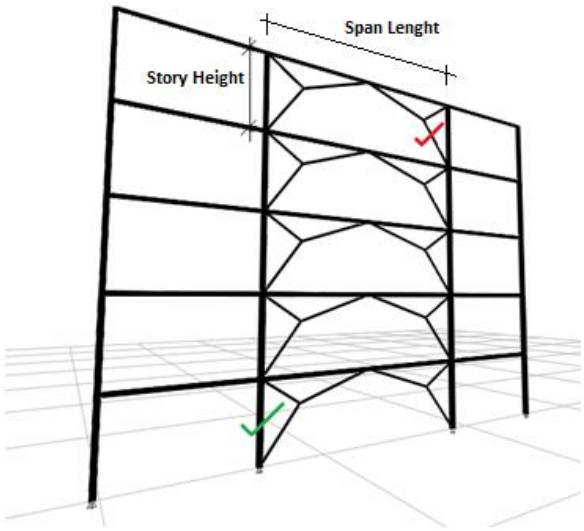

Figure 2. Gate Bracing Frame (GBF) in the current research, modelled with Sap2000

Three different ratios K in the bracing frame are included in the software modelling. The specifications of the types of frames are presented in Table (1). In the modelling, St37 steel was used in the structure, whose specifications are presented in Table (2).

Table 1. Typing of frames designed in the current research

Row	Left and right span length (m)	L = Middle span length (m)	h = Story height (m)	$K = \frac{L}{h}$
1	5	3	3	$K_1 = 1$
2	5	6	3	$K_2 = 2$
3	5	9	3	$K_3 = 3$

Table 2. Characteristics of St37 steel [49] in the modelling of steel structures

Parameter (Unit)	Minimum yield stress (Kg/cm^2)	Minimum tensile stress (Kg/cm^2)	Effective tensile stress (Kg/cm^2)	Effective tensile stress (Kg/cm^2)	Modulus of elasticity (GPa)	Poisson's ratio
Value	24×10^6	27×10^6	27.6×10^6	42.55×10^6	2.039×10^{10}	**0.3**

The ground under the structure has a high seismic risk (A=0.3) [50]. The usage type of the structure is residential (I=1) [50]. The soil under the structure is type III. The coefficient C (earthquake parameter) and the coefficient K (elevation parameter) have been calculated according to Iran standard 2800-fourth edition [51,52]. The seismic parameters of the structures are presented in Table (3).

Table 3. Seismic parameters of steel structures [50–52]

Frame Type	H (m)	T (Sec)	K	S	S_0	T_S (Sec)	T_0 (Sec)	B_1	N	B	C
5-Story	15	0.61	1	1.75	1.1	0.7	0.15	2.75	1	2.75	$C_{(R_u=3.5)} = 0.24$

H: structure total height, T: period time, B_1: spectrum shape factor, N: spectrum correction factor, B: building reflection factor, R_u: structure behavior factor and S, S_0 , T_S and T_0 are seismic parameters.

Structure loading includ1es gravity load (dead load equivalent to 500 kg/m and live load equivalent to 200 kg/m) [53] and lateral seismic load. By performing linear static analysis, members in 5-story steel frames were determined. Sections of members are presented in Table (4). All the frames were designed by LRFD method [53].

Table 4. Members details in a 5-story steel frames

Frame Type	Member	Desired Story	Section
5-Story	Beam	1-2	**IPE140**
		3-4	**IPE120**
		5	**IPE100**
	Brace	1-2	**TUBO60X30X5.9**
		3-4	**TUBO60X30X5**
		5	**TUBO60X30X4**
	Column	1-2	**HE180**
		3-4	**HE160**
		5	**HE140**

On January 17, 1995, a major earthquake with a magnitude of 7.2 struck near Kobe, Japan, causing significant damage and loss of life. The earthquake, known as the Great Hanshin Earthquake or the Kobe Earthquake, resulted in over 6,000 deaths and left more than 45,000 people homeless. The earthquake caused massive damage to Kobe Steel, a major Japanese steelmaker, which sustained 102 billion yen in damages. The company's Kobe Head Office was completely destroyed, and one of its blast furnaces had to be shut down. However, Kobe Steel managed to recover quickly, with the blast furnace back in operation just two and a half months later. The earthquake also had a significant impact on the structures, lifelines, and fire protection systems in the area. Traditional houses with heavy tiled roofs, which were designed to resist frequent typhoons, suffered serious structural damage when their wooden supports gave way, causing the roofs to crush the unreinforced walls and floors in a pancake collapse.

Newer homes with reinforced walls and lighter roofs were more susceptible to typhoons but less likely to experience the same level of damage [54,55]. The 1940 El Centro earthquake was a powerful seismic event that occurred on May 18, 1940, with a magnitude of 6.9 Mw and a depth of 16 km. It had a significant impact on the United States and Mexico, causing 6 million dollar in total damage and resulting in 9 deaths and 20 injuries. The earthquake was the result of a rupture along the Imperial Fault, with its epicenter 5 miles north of Calexico, California. A strong secondary earthquake with a magnitude of 5.5 followed a little more than an hour after the main event. In recent times, El Centro and its surrounding areas have experienced several smaller earthquakes. For example, a magnitude 3.7 earthquake was reported on December 5, 2023, occurring 16 miles from El Centro at a depth of 5.3 miles [55,56]. In present research, Dynamic analysis has been done with earthquakes in Kobe (near-fault) and El Centro (far-fault). Accelerometers of Kobe and El Centro are shown in Figures (3) and (4).

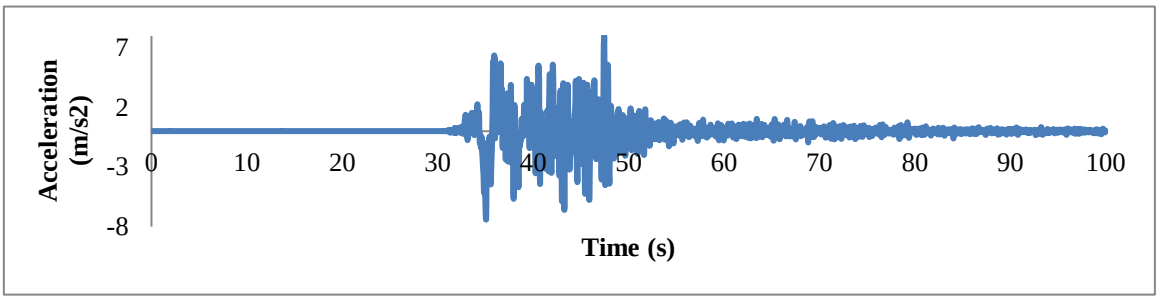

Figure 3. Accelerometer of the Kobe earthquake (near-fault) [57]

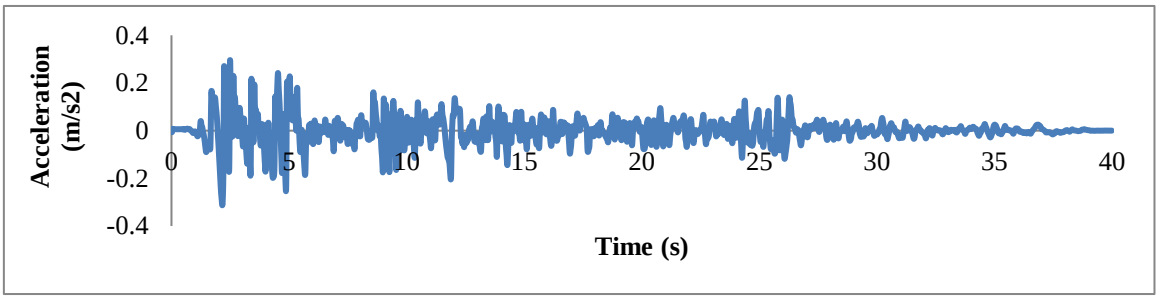

Figure 4. Accelerometer of the El Centro earthquake (far-fault) [58]

3. RESULTS AND DISCUSSION

3.1. Acceleration

In this section, the roof acceleration in the Kobe and El Centro earthquakes is presented. 10 seconds of peak acceleration changes are selected and presented in the acceleration-time graphs.

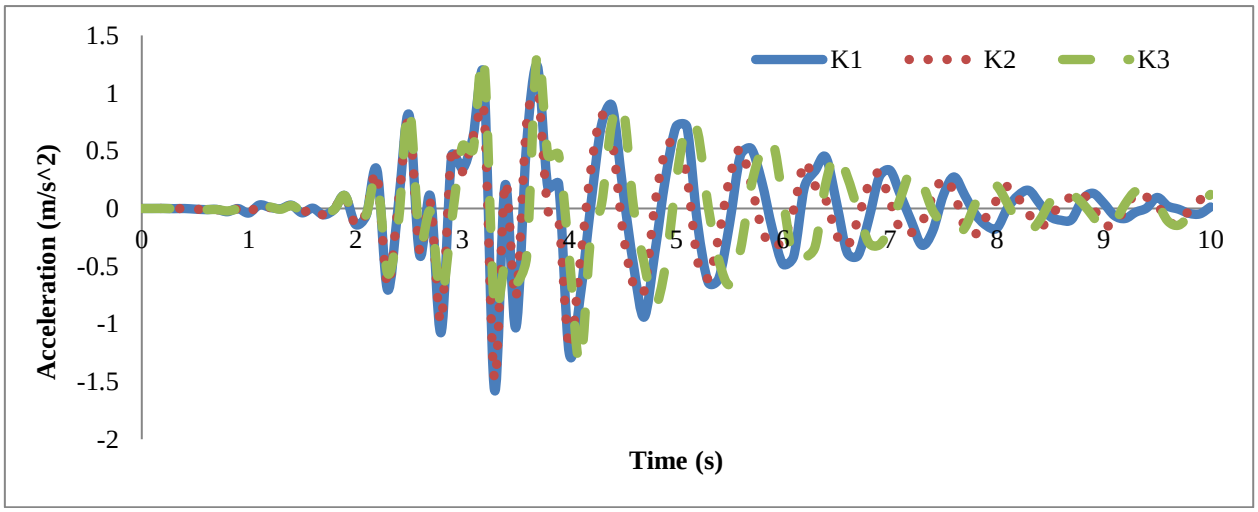

Figure 5. Acceleration-Time graph of the roof in 5-story steel structures with K1, K2 and K3 indexes under the Kobe earthquake

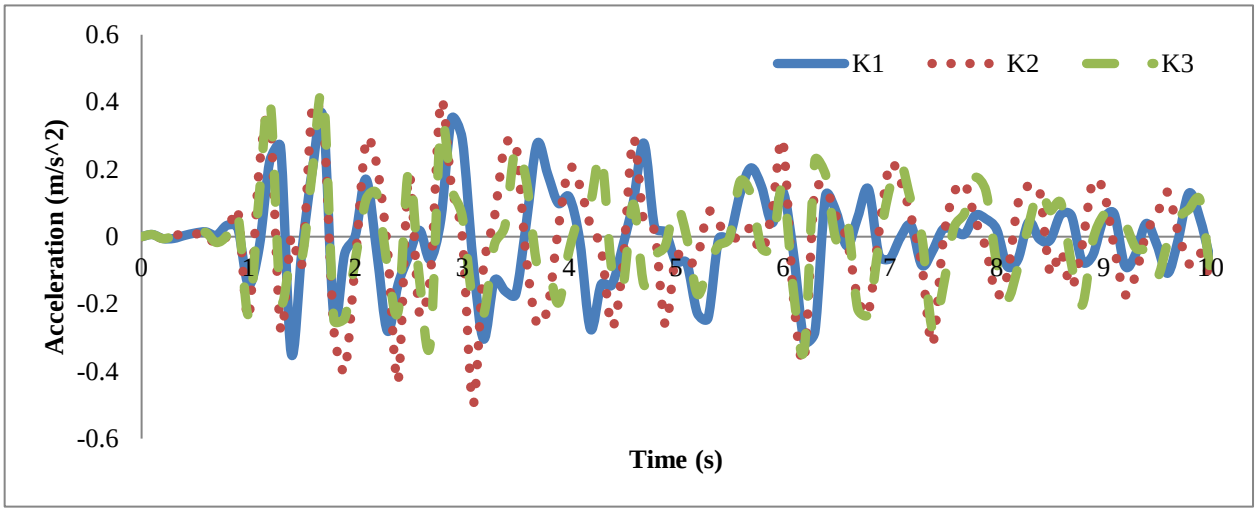

Figure 6. Acceleration-Time graph of the roof in 5-story steel structures with K1, K2 and K3 indexes under the El Centro earthquake

Figures (5) and (6) showed that increasing the K index does not necessarily increase the acceleration of the structure. At some times, the acceleration in the primary structure (with index K1) is higher than other structures. In Figures (7), the maximum gradient and the numerical average resulting from the modal dynamic analysis are presented. Figures (7) show that K2 index has the highest acceleration (maximum and average) compared to K1 and K3 indexes. The average acceleration in the K2 index is equal to 0.288 and 0.142 in the earthquakes of Kobe (near-fault) and El Centro (far-fault), respectively. Therefore, the average acceleration in near-fault earthquake is more than twice that of a far-fault earthquake. In K1 and K3 indexes, near-fault earthquakes have higher average acceleration compared to far-fault earthquakes.

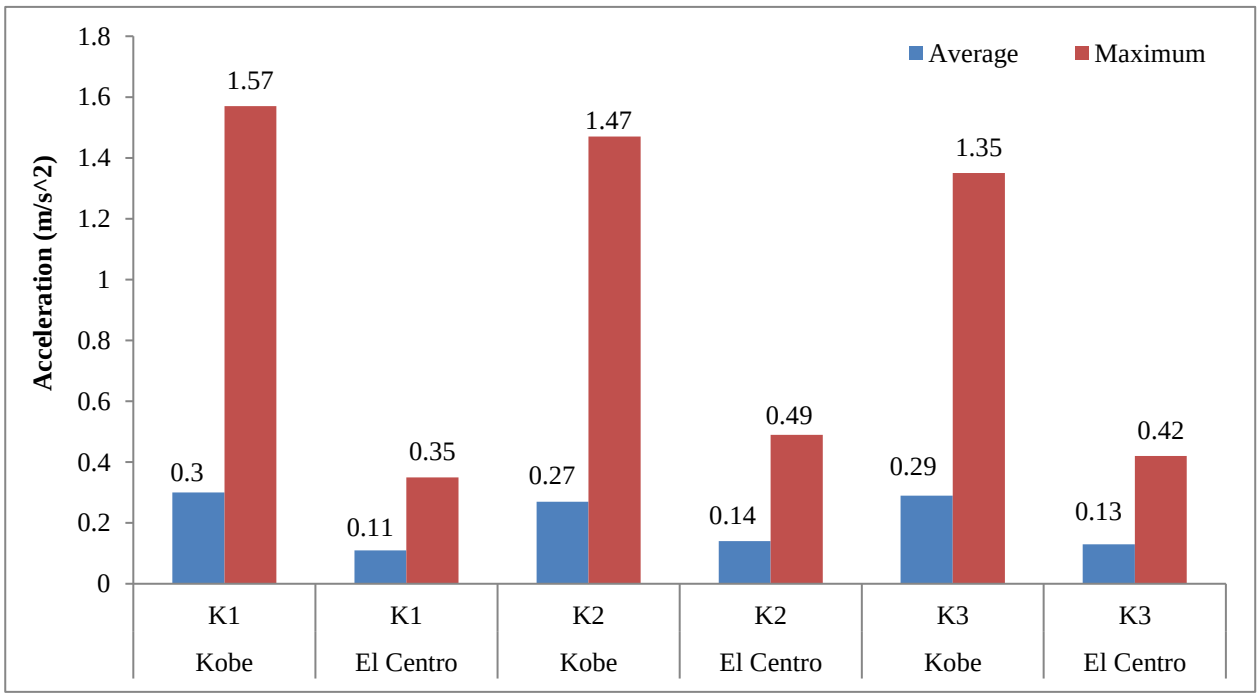

Figure 7. Average and maximum acceleration in 5-story steel structures with K1, K2 and K3 indexes under the Kobe and El Centro earthquakes

3.2. Modal Damping Energy

In this section, energy damping energy due to modal analysis is presented and compared in K1, K2 and K3 indexes. Also, equations and linear diagrams of Modal damping energy index are provided.

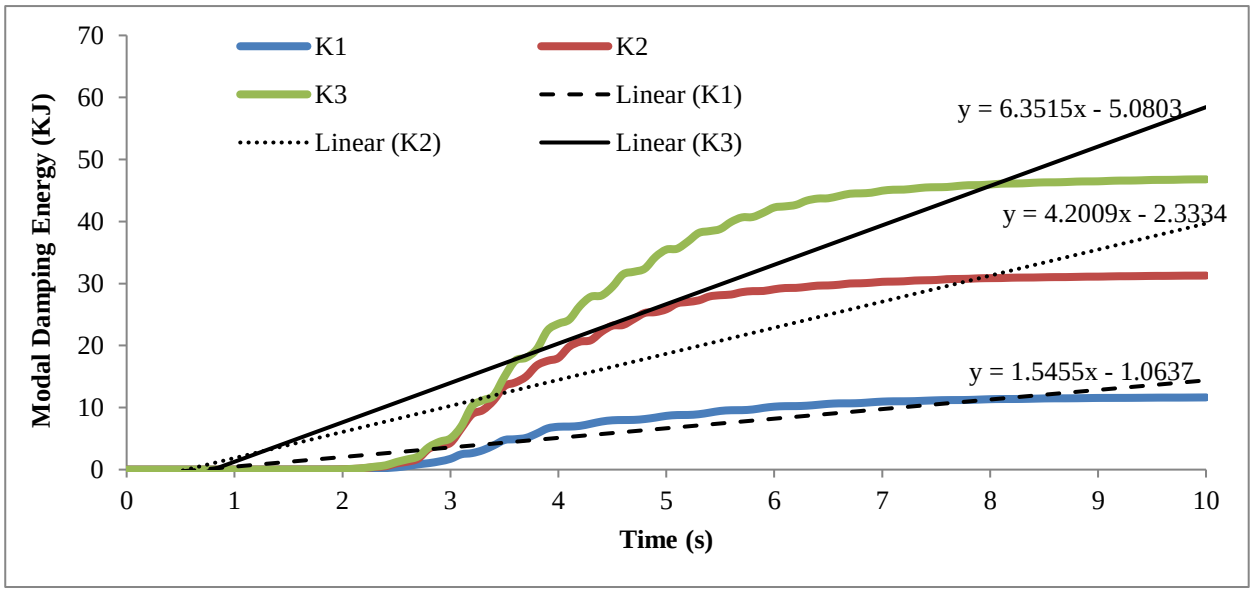

Figure 8. Modal damping energy in 5-story steel structures with K1, K2 and K3 indexes under the Kobe earthquake

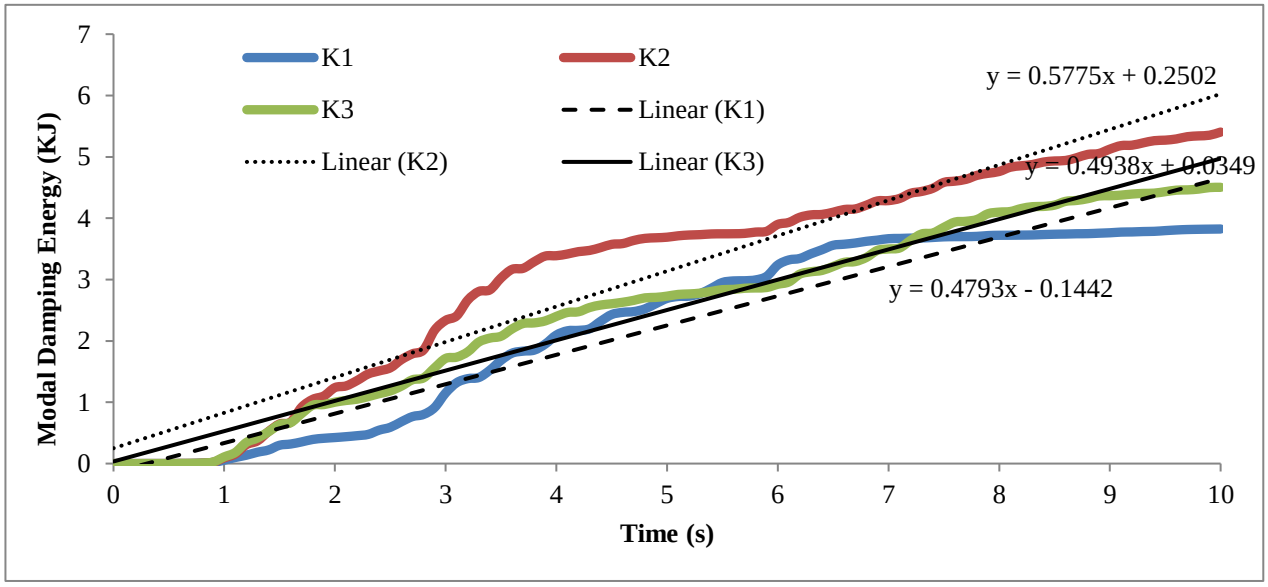

Figure 9. Modal damping energy in 5-story steel structures with K1, K2 and K3 indexes under the El Centro earthquake

The results showed that the value of Modal damping energy increases with the increase of K value. The slopes of the linear graphs K1, K2 and K3 are equal to 1.54, 4.2 and 6.35, respectively. The linear slope shows the influence of the K index on the increase of Modal damping energy. Figure (9) showed that increasing the K index of the far-fault area does not necessarily increase Modal damping energy. The results are different in the near-fault and far-fault areas. In the near-fault area, the relationship between K index and Modal damping energy is direct. In the far-fault area, there is no relationship between K index and Modal damping energy. Therefore, the distance between the location of the earthquake and the structure is very effective on the influence of the K index.

3.3. Base Shear Force

In this section, the base shear force in structures with indexes K1, K2 and K3 is presented.

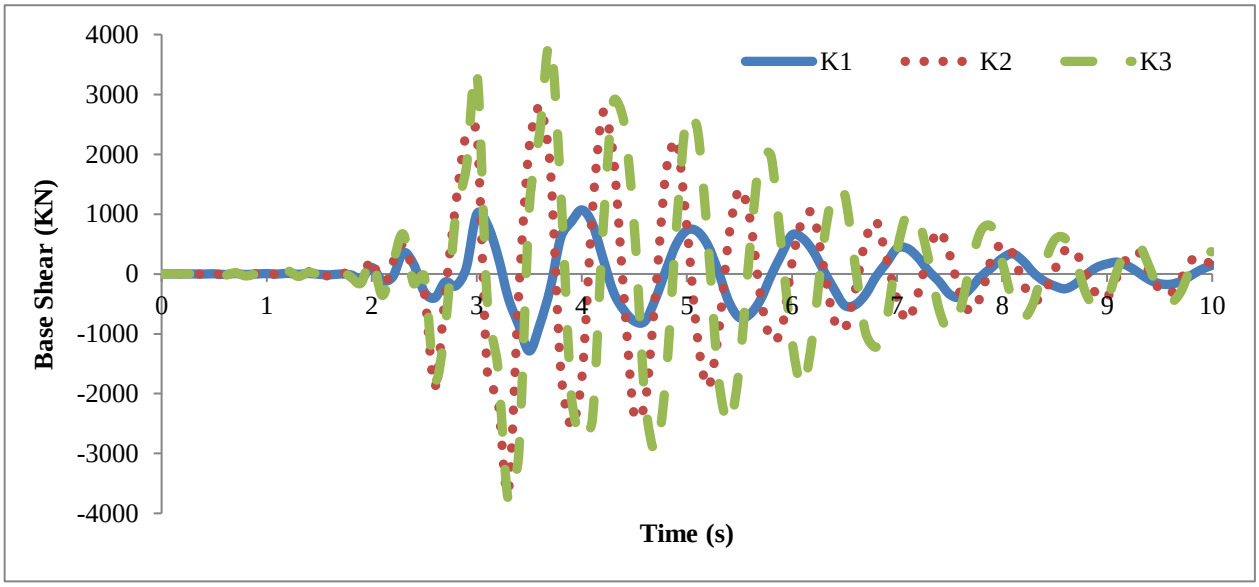

Figure 10. Base shear force in 5-story steel structures with K1, K2 and K3 indexes under the Kobe earthquake

Figure (10) showed that with the increase of the K index, the base shear force in the 5-story structure under the Kobe earthquake increases. The difference between the values of K1, K2 and K3 is very large. Therefore, the relationship between the increase of the K index and the base shear force in the near-fault area is direct. Figure (11) show that with the increase of the K index in the 5-story structure under the El Centro earthquake, unlike the Kobe earthquake, the base shear force does not necessarily increase. In some cases, the K2 index is greater than the K3 index, and the K1 index is always smaller than the K2 and K3 indexes. Therefore, it cannot be said with certainty that with the increase of the K index in the far-fault area, the base shear force increases.

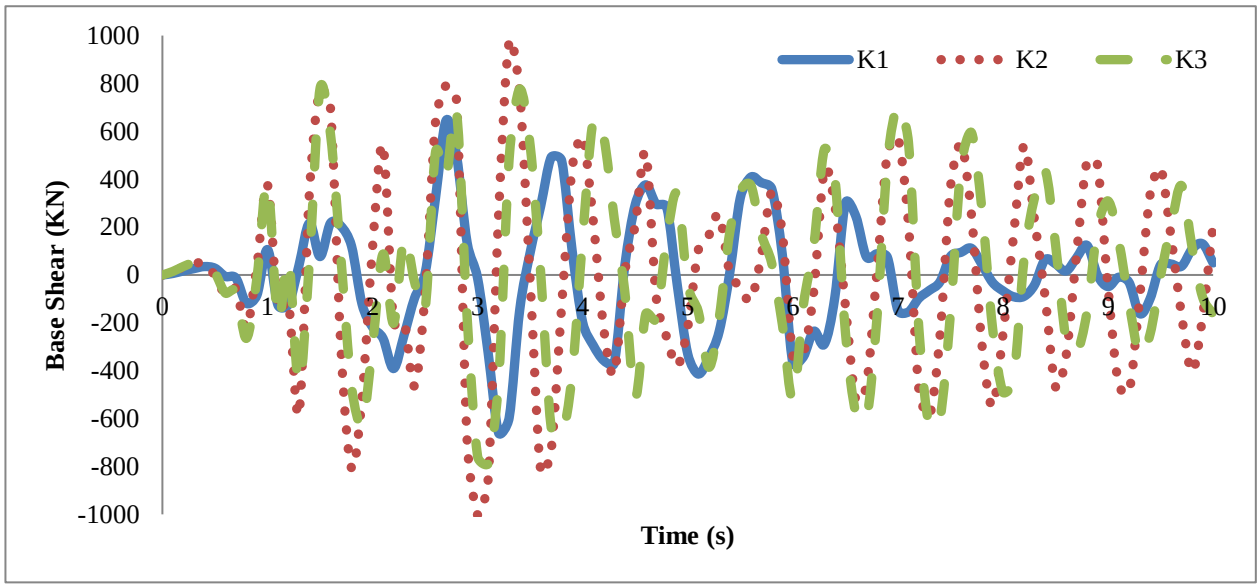

Figure 11. Base shear force in 5-story steel structures with K1, K2 and K3 indexes under the El Centro earthquake

3.4. Roof Displacement

In this section, the roof displacement with indexes K1, K2 and K3 is presented.

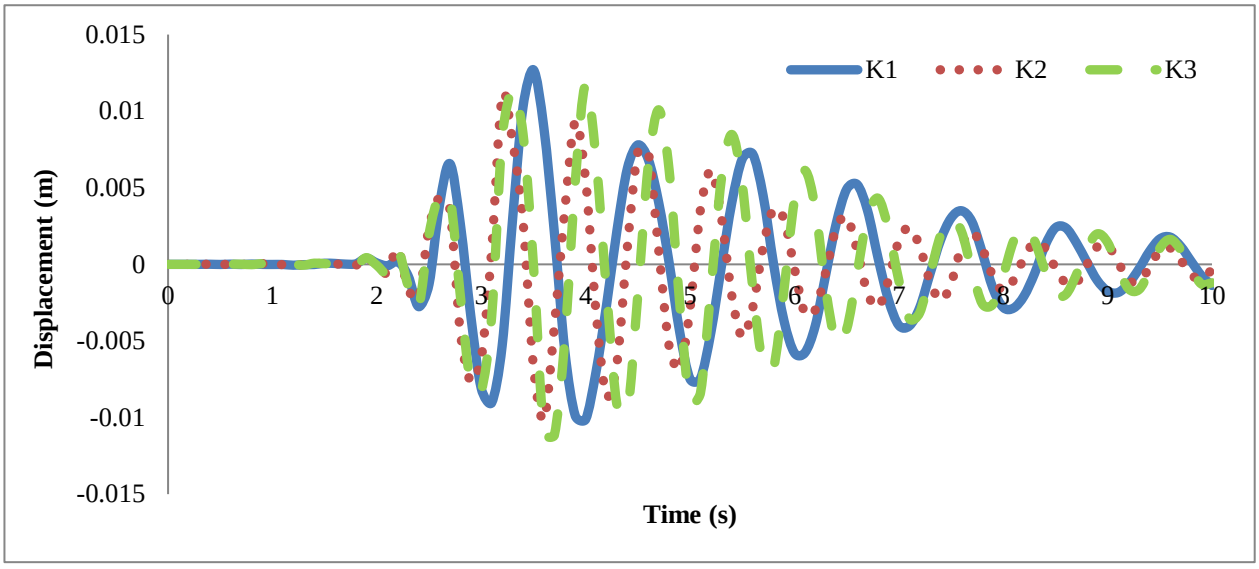

Figure 12. Roof displacement in 5-story steel structures with K1, K2 and K3 indexes under the Kobe earthquake

Figure (12) showed that in the near-fault area, there is no clear relationship between K index and Displacement. Most of the time, K1 index is higher than K2 and K3 indexes, and the increase in the span length did not increase the displacement of the structure. Figure (13) showed that there is no clear relationship between the changes of K index and Displacement. K1 index has more displacement compared to K2 and K3 indexes, but at some times (between 8 and 9 seconds), displacement in K3 index is more than K2. Therefore, there is no direct relationship between K and Displacement indexes in the far-fault area.

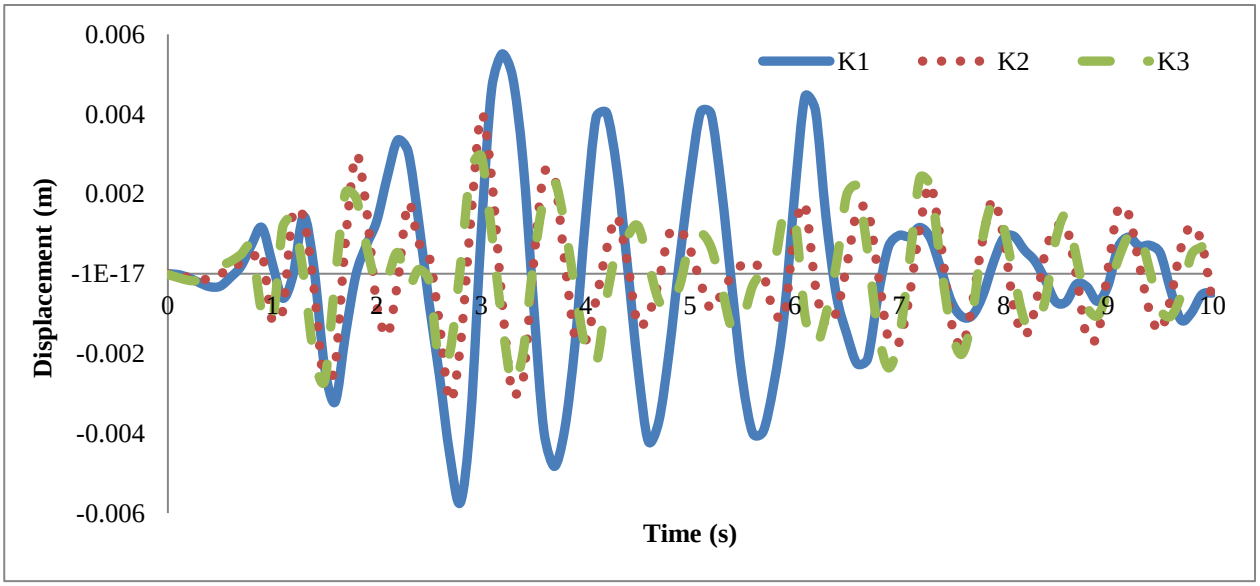

Figure 13. Roof displacement in 5-story steel structures with K1, K2 and K3 indexes under the El Centro earthquake

3.5. Axial Force in Bracing System

In this section, the axial force in the brace member (the element marked with a red tick in Figure 2) has been investigated. The axial force of the brace is also provided.

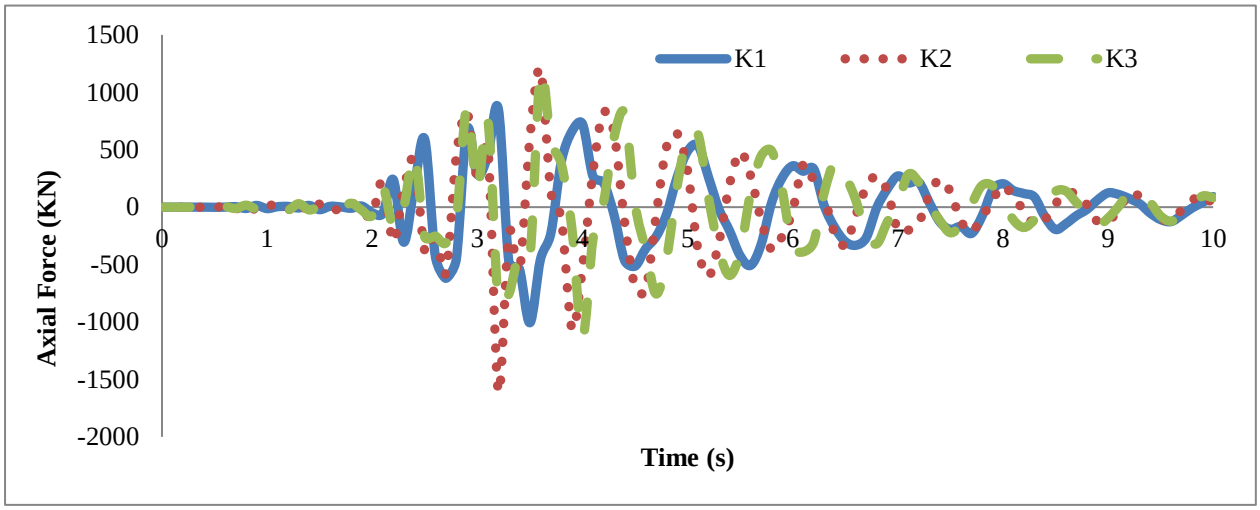

Figure 14. Axial Force in 5-story steel structures with K1, K2 and K3 indexes under the Kobe earthquake

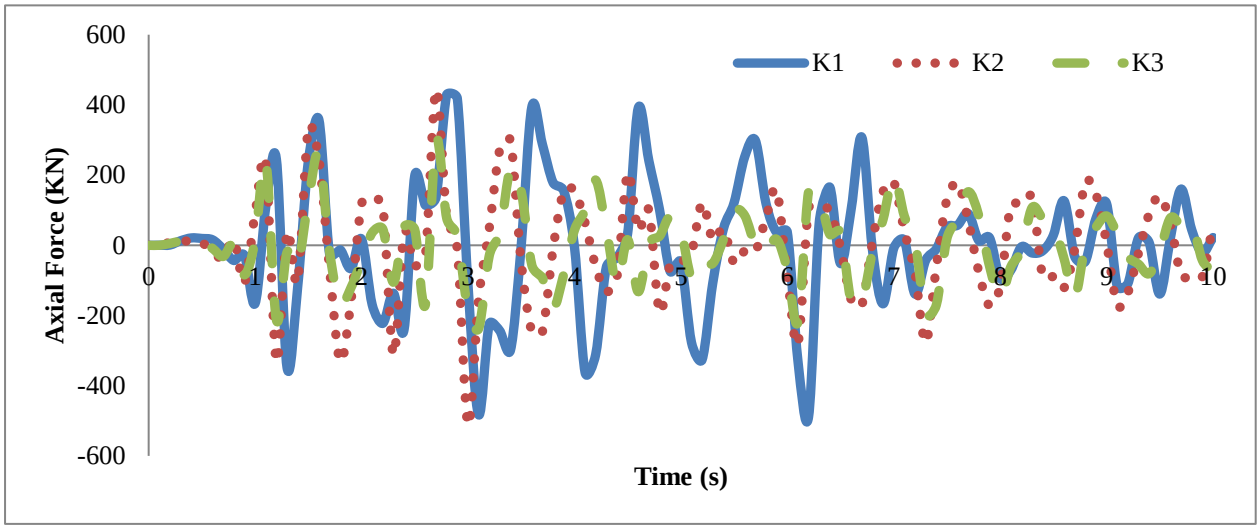

Figure 15. Axial Force in 5-story steel structures with K1, K2 and K3 indexes under the El Centro earthquake

Figures (14) and (15) show that there is no direct relationship between the K index and the axial force in the brace member in near and far-fault areas. In some times of loading the structure, an axial force in the structure with K2 and K3 indexes is more than the structure with K1 index. Therefore, the average and maximum axial force in the brace member is checked.

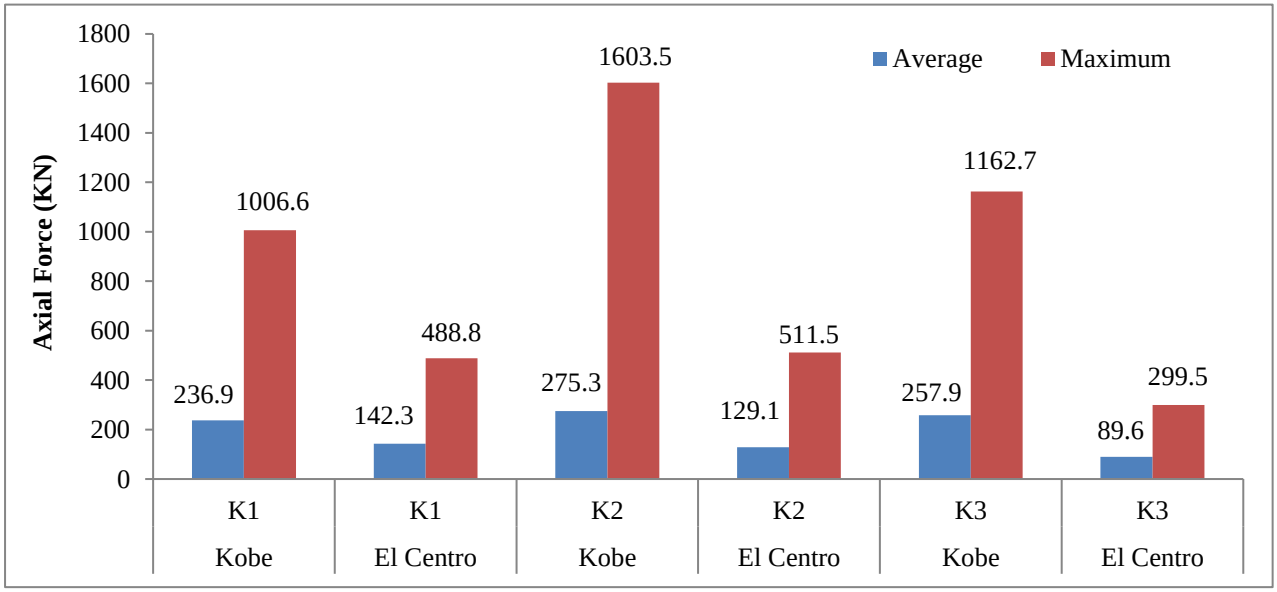

Figure 16. Axial Force in 5-story steel structures with K1, K2 and K3 indexes under the Kobe and El Centro earthquakes

Figure (16) showed that the increase of the K index in the steel frame does not necessarily increase an axial force of the brace, and this result exists in the near and far-fault area. The results showed that the K2 index, except for one case, has the highest axial force values compared to the K1 and K2 indexes.

3.6. Column Shear Force

In this section, the column shear force (the element marked with a green tick in Figure 2) has been investigated. Also, the numerical values of the average and maximum of columns shear force are presented.

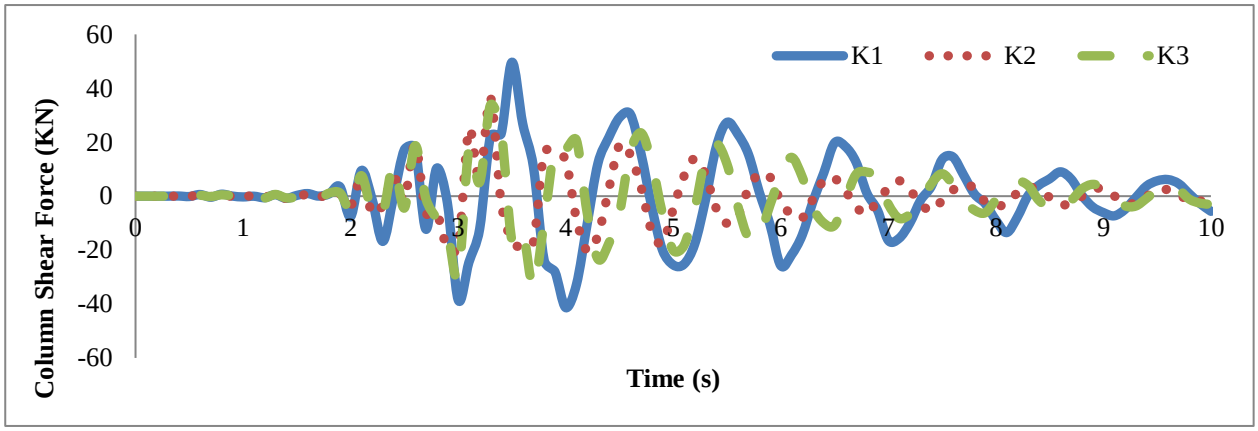

Figure 17. Column shear force in 5-story steel structures with indexes K1, K2 and K3 under the Kobe earthquake

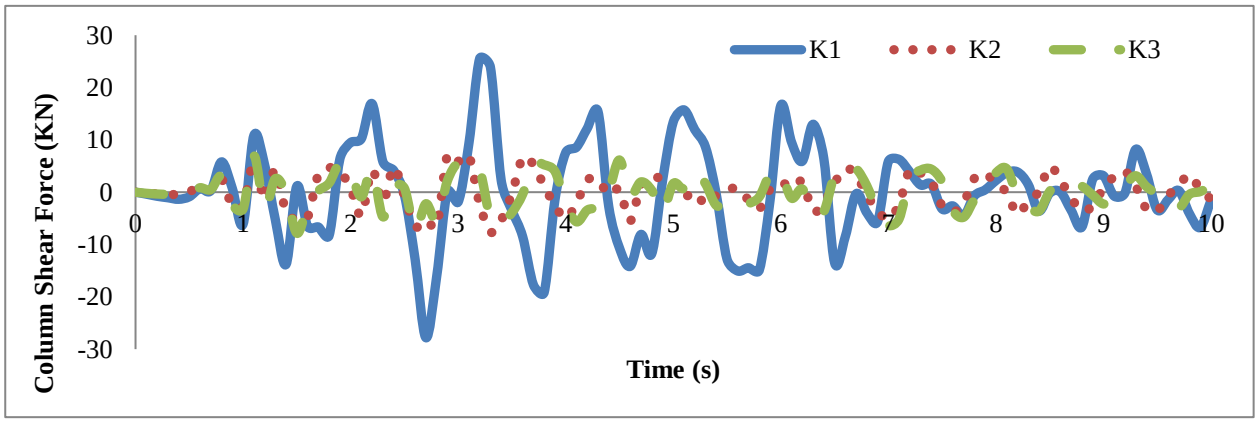

Figure 18. Column shear force in 5-story steel structures with K1, K2 and K3 indexes under the El Centro earthquake

Figures (17) and (18) showed that the structure with index K1 has the highest column shear force in the near- fault and far-fault areas. Column shear forces in structures with indexes K2 and K3 are close to each other. Figure (19) shows the average and maximum shear force in the column.

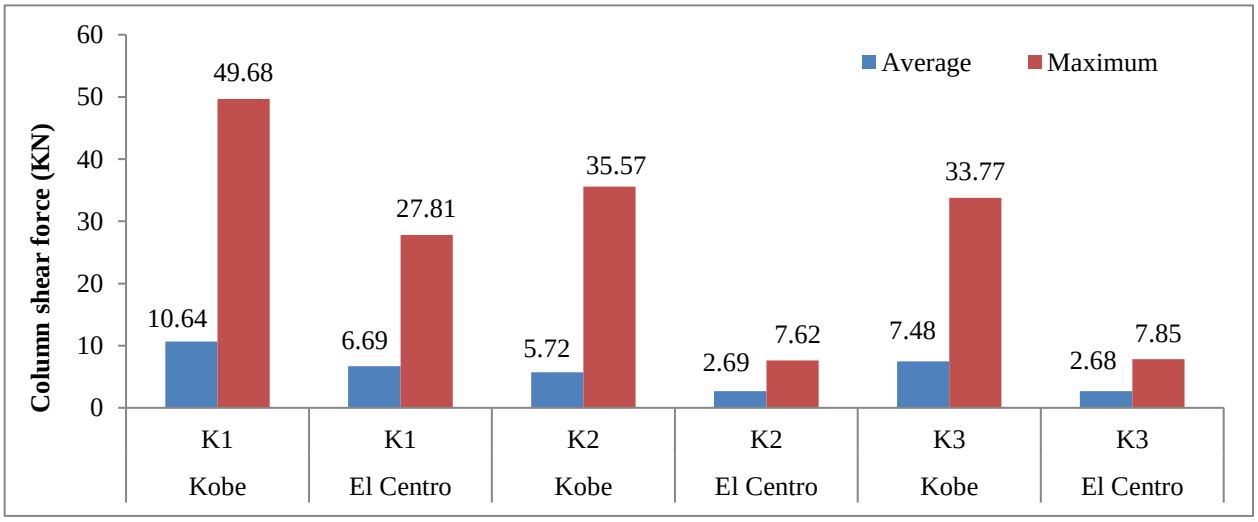

Figure 19. Column shear force in 5-story steel structures with K1, K2 and K3 indexes under the Kobe and El Centro earthquakes

3.7. Support Reaction Force

In this section, the maximum support force in a 5-story steel structure is presented. Also, the average and maximum numerical values of the support reaction force are provided.

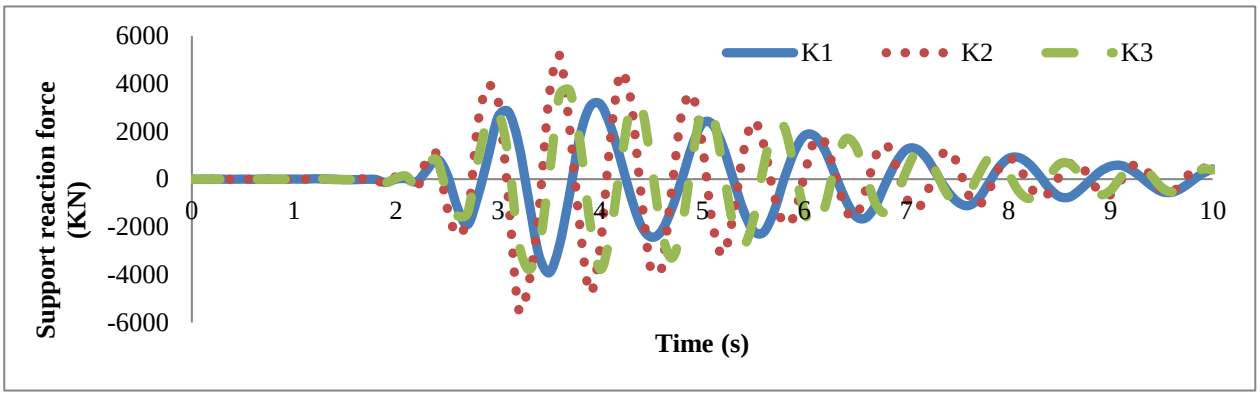

Figure 20. Support reaction force in 5-story steel structures with K1, K2 and K3 indexes under the Kobe earthquake

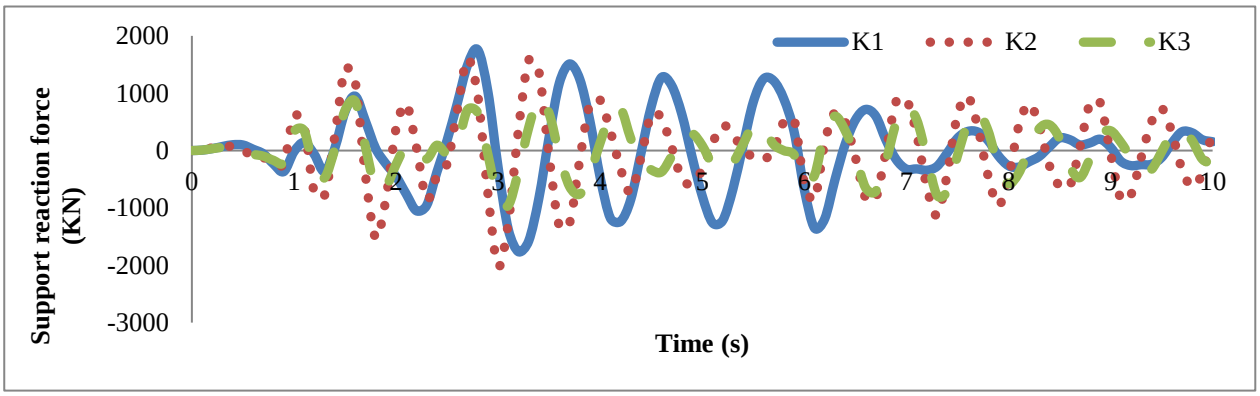

Figure 21. Support reaction force in 5-story steel structures with K1, K2 and K3 indexes under the El Centro earthquake

Figures (20) and (21) showed that the structure with index K2 has the highest support reaction force. Also, increasing the value of the K index does not necessarily increase the support reaction force. These results exist in both near and far-fault areas. In Figure (22), the average and maximum support reaction forces in different K indexes are presented.

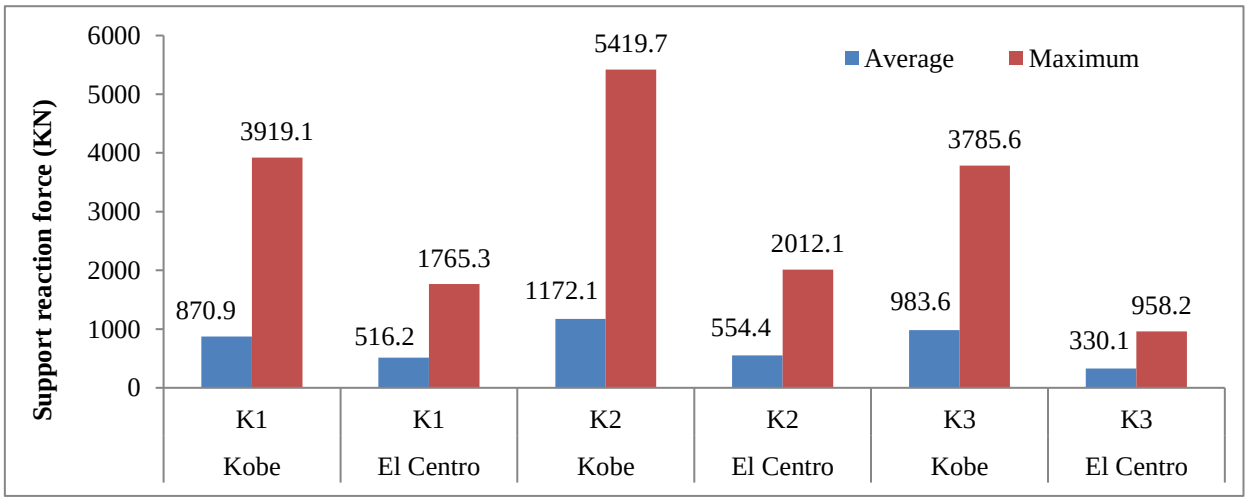

Figure 22. Support reaction force in 5-story steel structures with K1, K2 and K3 indexes under the Kobe and El Centro earthquakes

Figure (22) showed that the index placement order is as follows: (a) K2, (b) K1 and (c) K3. Therefore, increasing the K index does not necessarily increase the support reaction force.

3.8. Story Displacement

In this section, the Story displacement in the near and far-fault areas is presented.

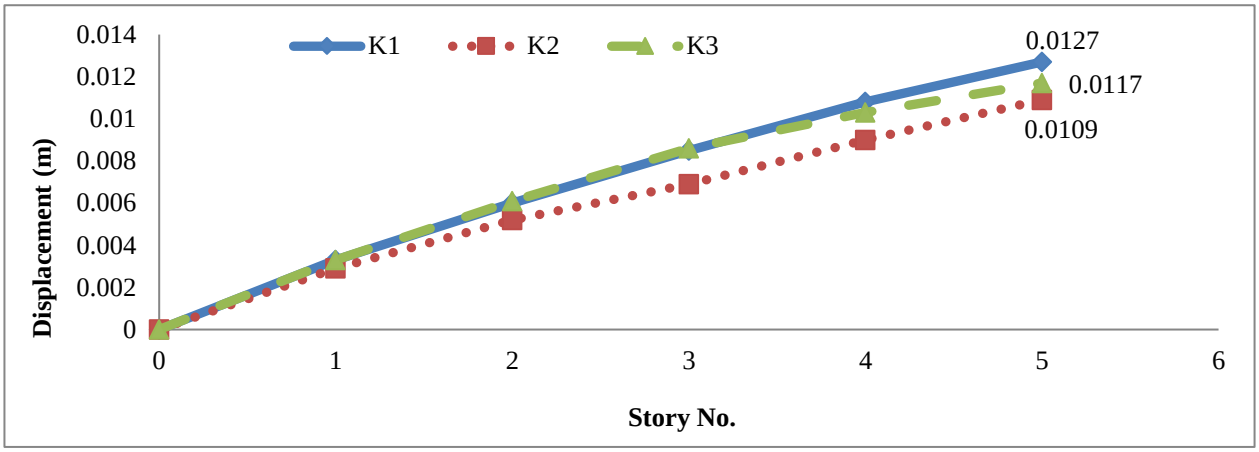

Figure 23. Story displacement in 5-story steel structures with K1, K2 and K3 indexes under the Kobe earthquake

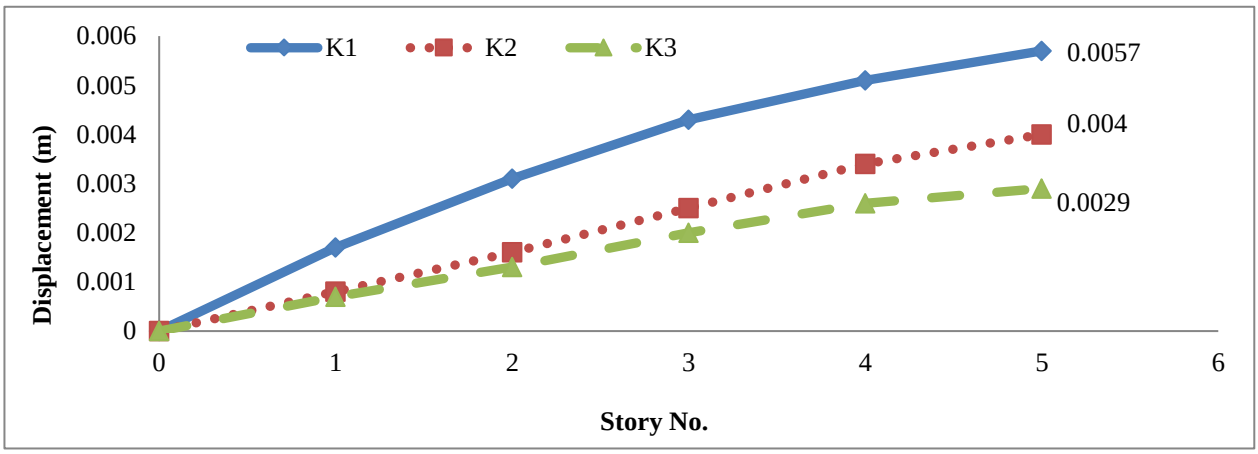

Figure 24. Story displacement in 5-story steel structures with K1, K2 and K3 indexes under the El Centro earthquake

Figures (23) and (24) showed that the structure with index K1 has the most story displacement (in near and far-fault areas). In the Kobe earthquake (near-fault area), the story displacement in with K3 index is more than K2 index. In the far-fault area (El Centro earthquake), the story displacement with K2 index is more than K3 index. Therefore, the increase in the K index and the story displacement in the near and far-fault areas are not directly related.

3.9. Discussion

Geometric dimensions have a great impact on the seismic performance of the structure. In many studies, the effect of geometric characteristics is only related to the dimensions of beams and columns. Many structural parameters, such as design forces of members, depend on the span length and the story height. In the current research, the K index is defined as dividing span length by story height. Three different ratios of K equivalent to 1, 2 and 3 are defined. To perform modal time history analysis, near-fault earthquake (Kobe) and far-fault earthquake (El Centro) have been used. In many researches, including [59–65], the effect of near and far-fault earthquakes on the structure has been investigated. Investigating the effect of the geometrical dimensions of the structure in the near-fault and far-fault areas has rarely been investigated in studies, which has been fully investigated in the present research. The results obtained from the present research showed that modal damping energy and base shear force indexes have a direct relationship with the K index. This result exists only in the near-fault area. In Sadeghpour et al. [66] research, it was stated that the arrangement of elements in the structure causes many changes in the behavior coefficient and the base shear force.

Therefore, it confirms the results of the current research and presents the effect of geometric characteristics on the seismic performance of the structure. Vikas and Chey [67] investigated the seismic performance of RC structure with geometrical irregularities. They obtained results that confirm the results of the present study.

4. CONCLUSION

There is no direct relationship between the K index and the acceleration of the structure. This result is valid in areas near-fault and far-fault. Therefore, the increase or decrease of the K index cannot be used as a criterion to check the acceleration of the structure.

In the near-fault area, according to the magnitude of the applied earthquake, the modal damping energy is influenced by the K index. Therefore, the K index and modal damping energy are directly related, and increasing the K index causes a great increase in modal damping energy in the structure. Also, decreasing the K index causes a decrease in modal damping energy in the structure. In the far-fault area, due to the reduction of applied earthquake magnitude, modal damping energy is not affected by the K index. The results showed that increasing the K index has caused changes, but it has no direct relationship with modal damping energy. Therefore, it can be said that in the near-fault area, K index and modal damping energy have a direct relationship, and in the far-fault area, K index and modal damping energy do not have a direct relationship.

In the near-fault area, the K index and the base shear force in the structure have a direct relationship. This result is due to the large magnitude of the earthquake in the near-fault area. In the far-fault area, there is no direct relationship between the K index and the base shear force in the structure.

In the near and far-fault areas, the K index and the roof displacement are not directly related. Therefore, changes in the K index do not cause specific changes in the roof displacement.

In near and far-fault areas, the K index and the axial force in the gate brace system do not have a direct relationship. Therefore, changes in K index do not cause specific changes in the near-fault area. The increase in the K index causes an increase in the average axial force in the gate brace system. In the far-fault area, due to the small magnitude of the earthquake, the increase in the K index causes a decrease in the average axial force in the gate brace system.

The K index and the column shear force are not directly related in the near and far-fault areas. Changes in the K index do not cause specific changes in the column shear force.

K index and support reaction force are not directly related in near and far-fault areas. In the near-fault area, due to the high Richter magnitude of the earthquake, increasing the index K causes an increase in the support reaction force. In the far-fault area, due to the low power of the earthquake on the structure, increasing the K index does not cause a specific change in the support reaction force of the structure.

The K index and the story displacement, in the near and far-fault area, do not have a direct relationship. In the near-fault area, due to the magnitude of the earthquake's Richter scale, the increase in the K index causes a decrease in the story displacement. This trend also exists in the far-fault area with less intensity.

FUNDING/SUPPORT
Not mentioned any Funding/Support by authors.

ACKNOWLEDGMENT
Not mentioned by authors.

AUTHORS CONTRIBUTION
This work was carried out in collaboration among all authors.

ONFLICT OF INTEREST
The author (s) declared no potential conflicts of interests with respect to the authorship and/or publication of this paper.

5. REFERENCES

[1] Jing F, Zhang L, Singh RP, Chauhan A, Jiang M. Quasi-coseismic variations and geosphere coupling associated with the strong 2023 Turkey earthquakes. Science of The Total Environment. 2024 Jan 10;907:167963. [View at Google Scholar]; [View at Publisher].

[2] Zuo K, Zhao C. Seismicity and seismogenic mechanism of the MS 6.0 Luxian earthquake on September 16, 2021. Earthquake Research Advances. 2023 Oct 1;3(4):100253. [View at Google Scholar]; [View at Publisher].

[3] Chiba K. Spatiotemporal variations in seismic activity in and around the focal region of the 2021 M7. 3 and 2022 M7. 4 Fukushima-Oki earthquakes, Japan. Tectonophysics. 2024 Jan 9;870:230150. [View at Google Scholar]; [View at Publisher].

[4] Wang X, Zhao C. Rupture process of the January 8, 2022, Menyuan M 6.9 earthquake. Earthquake Research Advances. 2023 Oct 1;3(4):100268. [View at Google Scholar]; [View at Publisher].

[5] Zhao Q, Jiang F, Zhu L, Xu J. Synthetic aperture radar interferometry–based coseismic deformation and slip distribution of the 2022 Menyuan MS6. 9 earthquake in Qinghai, China. Geodesy and Geodynamics. 2023 Nov 1;14(6):541-50. [View at Google Scholar]; [View at Publisher].

[6] Mahto P, Gupta SC. Tectonic stress regime and faulting style analysis due to sequence of earthquakes in Western Nepal. Natural Hazards Research. 2023 Nov 23. [View at Google Scholar]; [View at Publisher].

[7] Zi J, Yang H, Su J, Chen L. Structural constraints of induced earthquakes in the Weiyuan Shale Gas Field revealed by high-resolution body-wave tomography and earthquake relocation. Tectonophysics. 2023 Oct 5;864:230007. [View at Google Scholar]; [View at Publisher].

[8] Lou T, Wang W, Izzuddin BA. System-level analysis of a self-centring moment-resisting frame under post-earthquake fire. Engineering Structures. 2023 Aug 15;289:116294. [View at Google Scholar]; [View at Publisher].

[9] Tena-Colunga A, Sánchez-Ballinas D. The collapse of Alvaro Obregon 286 building in Mexico City during the September 19, 2017 earthquake. A case study. Journal of Building Engineering. 2022 May 15;49:104060. [View at Google Scholar]; [View at Publisher].

[10] Li CY, Lin CH, Chang CW, Chuang CH, Chung YH, Hu MH, Lin CL. Musculoskeletal injuries and management of victims from collapsed buildings in the 2016 Taiwan earthquake: experiences in a tertiary medical center. Injury. 2021 Nov 1;52(11):3334-9.. [View at Google Scholar]; [View at Publisher].

[11] Torghabeh AB, Tehranizadeh M, Taslimi A. Probability of collapse evaluation for high-rise reinforced concrete buildings in the event of near-fault earthquakes and soil-structure interaction effects. InStructures 2023 Sep 1 (Vol. 55, pp. 1675-1691). Elsevier. [View at Google Scholar]; [View at Publisher].

[12] Guo M, Ge X, Wang S. Slope stability analysis under seismic load by vector sum analysis method. Journal of Rock Mechanics and Geotechnical Engineering. 2011 Sep 25;3(3):282-8. [View at Google Scholar]; [View at Publisher].

[13] Chatterjee K, Choudhury D, Poulos HG. Seismic analysis of laterally loaded pile under influence of vertical loading using finite element method. Computers and Geotechnics. 2015 Jun 1;67:172-86. [View at Google Scholar]; [View at Publisher].

[14] Zhang C, Duan C, Sun L. Experimental investigation of FPS inter-storey isolation control for assembled steel structure with high aspect ratio. InStructures 2023 Jul 1 (Vol. 53, pp. 550-567). Elsevier. [View at Google Scholar]; [View at Publisher].

[15] Majima R, Hayashi K, Saito T. Development of new passive vibration control system in coupled structures with block and tackle. Soil Dynamics and Earthquake Engineering. 2022 Aug 1;159:107319. [View at Google Scholar]; [View at Publisher].

[16] Sarmeili M, Ashtiani HR, Rabiee AH. Nonlinear energy sinks with nonlinear control strategies in fluid-structure simulations framework for passive and active FIV control of sprung cylinders. Communications in Nonlinear Science and Numerical Simulation. 2021 Jun 1;97:105725. [View at Google Scholar]; [View at Publisher].

[17] Yao H, Tan P, Zhou H, Zhou F. Real-time hybrid testing for active mass driver system based on an improved control strategy against control-structure-interaction effects. Journal of Building Engineering. 2023 Jan 1;63:105477. [View at Google Scholar]; [View at Publisher].

[18] Almeida DI, Cárdenas AC, Fuentes IO, Cota RC, León LO, Martínez DR, Contreras AM. Modeling and control of an invasive mechanical ventilation system using the active disturbances rejection control structure. ISA transactions. 2022 Oct 1;129:345-54. [View at Google Scholar]; [View at Publisher].

[19] Farahpour H, Hejazi F. Development of integrated semi-active adaptive vibration control system for bridges subjected to traffic loads. InStructures 2023 May 1 (Vol. 51, pp. 1773-1794). Elsevier. [View at Google Scholar]; [View at Publisher].

[20] Lian H, Sun X, Lian Y, Xie L, Yu Z. Strain rate effect on the fracture parameters of concrete three-point bending beam with a small span-to-height ratio. Engineering Fracture Mechanics. 2023 Mar 28;281:109133. [View at Google Scholar]; [View at Publisher].

[21] Takadate Y, Uematsu Y. Aerodynamic stability and vibration mechanism of long-span flat roofs with various span to eaves-height ratios. Journal of Wind Engineering and Industrial Aerodynamics. 2023 Sep 1;240:105494. [View at Google Scholar]; [View at Publisher].

[22] Li X, Zhang Z, Xue S, Yanli H. Experimental and simulation analysis of the initial shape of a large-span air-supported membrane structure. Thin-Walled Structures. 2022 Sep 1;178:109491. [View at Google Scholar]; [View at Publisher].

[23] Meng B, Xiong Y, Zhong W, Li C, Li H. Collapse resistance analysis of steel frame structures with varying spans using component models. InStructures 2023 Nov 1 (Vol. 57, p. 105255). Elsevier.. [View at Google Scholar]; [View at Publisher].

[24] Pham AT, Lim NS, Tan KH. Experimental investigation on alternate load path mechanisms in double-span beams with unsymmetrical span lengths and reinforcement ratios. InStructures 2023 Oct 1 (Vol. 56, p. 105017). Elsevier. [View at Google Scholar]; [View at Publisher].

[25] Embaby K, El Naggar MH, El-Sharnouby M. Ultimate capacity of large-span soil-steel structures. Tunnelling and Underground

Space Technology. 2023 Feb 1;132:104887. [View at Google Scholar]; [View at Publisher].

[26] Yu Y, Fang H. A material-component-structure coupling damage model for the cyclic elastoplastic design of a large-span photovoltaic structure. Ocean Engineering. 2023 Dec 1;289:116299. [View at Google Scholar]; [View at Publisher].

[27] Gao K, Huang H, Zou Z, Wu Z, Zhu H, Yang J. Buckling analysis of multi-span non-uniform beams with functionally graded graphene-reinforced foams. International Journal of Mechanical Sciences. 2024 Feb 1;263:108777. [View at Google Scholar]; [View at Publisher].

[28] Ci MY, Sun HY, Qiao DH, Feng WH, Wang RC, Wang SJ. Effect of axial-load ratio and shear-span ratio on seismic behavior of the prefabricated structures for cast-in-place RC boundary elements confined uniform hollow panels. Journal of Building Engineering. 2023 Dec 1;80:108053. [View at Google Scholar]; [View at Publisher].

[29] Artar M, Carbas S. Optimum sizing design of steel frame structures through maximum energy dissipation of friction dampers under seismic excitations. InStructures 2022 Oct 1 (Vol. 44, pp. 1928-1944). Elsevier. [View at Google Scholar]; [View at Publisher].

[30] Kalilzadeh Vahidi E, Chavoshani P. The effect of increasing span length and storey height on the progressive failure of reinforced concrete frames with different percentages of openings in the masonry infilled wall. Journal of Structural and Construction Engineering. 2021 May 22;8(Special Issue 1):431-47. [View at Google Scholar]; [View at Publisher].

[31] Zheng Z, Bai Y. Effects of impact loads on mechanical performance for truss structure. World J Eng Technol. 2017 Aug 11;5:135-40. [View at Google Scholar]; [View at Publisher].

[32] Wang W, Zhang D, Lu F, Wang SC, Tang F. The effect of span length to height ratio of reinforced concrete slabs on pressure-impulse diagram with multiple failure modes under blast loading. InEPJ Web of Conferences 2012 (Vol. 26, p. 04015). EDP Sciences. [View at Google Scholar]; [View at Publisher].

[33] Rezvani FH, Yousefi AM, Ronagh HR. Effect of span length on progressive collapse behaviour of steel moment resisting frames. InStructures 2015 Aug 1 (Vol. 3, pp. 81-89). Elsevier. [View at Google Scholar]; [View at Publisher].

[34] Nicol A, Walsh J, Childs C, Manzocchi T. The growth of faults. InUnderstanding faults 2020 Jan 1 (pp. 221-255). Elsevier. [View at Google Scholar]; [View at Publisher].

[35] Brandes C, Tanner DC. Fault mechanics and earthquakes. InUnderstanding Faults 2020 Jan 1 (pp. 11-80). Elsevier. [View at Google Scholar]; [View at Publisher].

[36] Altunışık AC, Sunca F, Sevim B. Modal parameter identification and seismic assessment of historical timber structures under near-fault and far-fault ground motions. InStructures 2023 Jan 1 (Vol. 47, pp. 1624-1651). Elsevier. [View at Google Scholar]; [View at Publisher].

[37] Bilgin H. Effects of near-fault and far-fault ground motions on nonlinear dynamic response and seismic damage of masonry structures. Engineering Structures. 2024 Feb 1;300:117200. [View at Google Scholar]; [View at Publisher].

[38] Labibzadeh M, Khayat M. Damage assessment of stiffened steel plate shear walls with different configurations under far-fault and near-fault ground motions. Journal of Constructional Steel Research. 2023 Jan 1;200:107685. [View at Google Scholar]; [View at Publisher].

[39] Wu K, Ma J, Chuai M, Li CH, Chen Y, Lv F. Numerical simulation of the near-fault spontaneous rupture and its influence on dynamic soil-structure interaction. InStructures 2022 Apr 1 (Vol. 38, pp. 808-819). Elsevier. [View at Google Scholar]; [View at Publisher].

[40] Pemmasani V, Mareddy K, Vemuri J, Subramaniam KV. Time-frequency analysis of ground motions from the 1999 Chamoli earthquake. InMulti-Hazard Vulnerability and Resilience Building 2023 Jan 1 (pp. 233-247). Elsevier. [View at Google Scholar]; [View at Publisher].

[41] Stein S, Wysession M. An introduction to seismology, earthquakes, and earth structure. John Wiley & Sons; 2009 Apr 1. [View at Google Scholar]; [View at Publisher].

[42] Guo P, Zhao H, Xiang P, Liu X, Tan J, Jiang L. Probabilistic analysis of high-speed train safety on bridges under stochastic near-fault pulse-type ground motions. Probabilistic Engineering Mechanics. 2023 Oct 1;74:103527. [View at Google Scholar]; [View at Publisher].

[43] Li J, Xu L. Seismic performance improvement of continuous rigid-frame bridges with hybrid control system under near-fault ground motions. Soil Dynamics and Earthquake Engineering. 2023 May 1;168:107858. [View at Google Scholar]; [View at Publisher].

[44] Kumar P, Joshi A. Emerging techniques to simulate strong ground motion. InBasics of Computational Geophysics 2021 Jan 1 (pp. 33-46). Elsevier. [View at Google Scholar]; [View at Publisher].

[45] de Souza GF, Caminada Netto A, de Andrade Melani AH, de Carvalho Michalski MA, da Silva RF. Chapter 5: Engineering systems fault detection methods. Reliability Analysis and Asset Management of Engineering Systems, Advances in Reliability Science. 2022:119. [View at Google Scholar]; [View at Publisher].

[46] Lisle R, Orife T, Arlegui L. A stress inversion method requiring only fault slip sense. Journal of Geophysical Research: Solid Earth. 2001 Feb 10;106(B2):2281-9. [View at Google Scholar]; [View at Publisher].

[47] Gerami M, Abdollahzadeh D. Local and global effects of forward directivity. Građevinar. 2013 Dec 12;65(11.):971-85. [View at Google Scholar]; [View at Publisher].

[48] Hu K, Yang Y, Mu S, Qu G. Study on High-rise Structure with Oblique Columns by ETABS, SAP2000, MIDAS/GEN and SATWE. Procedia engineering. 2012 Jan 1;31:474-80. [View at Google Scholar]; [View at Publisher].

[49] Benli B, Celik I. Surface Modification and Analysis of St37 Steel with Al2O3-TiO2, ZrO2, and Cr2O3 Ceramic Coatings: Structural, Mechanical, and Tribological Properties. Tribology International. 2024 Mar 1;191:109183. [View at Google Scholar]; [View at Publisher].

[50] Zarrineghbal A, Zafarani H, Rahimian M. Towards an Iranian national risk-targeted model for seismic hazard mapping. Soil Dynamics and Earthquake Engineering. 2021 Feb 1;141:106495. [View at Google Scholar]; [View at Publisher].

[51] Moghaddam H, Darbani MS, Sadrara A, Hajirasouliha I. Recommendation of new design spectra for Iran using modified

Newmark method. Soil Dynamics and Earthquake Engineering. 2024 Jan 1;176:108332. [View at Google Scholar]; [View at Publisher].

[52]Mansouri S, Kontoni DP, Pouraminian M. The effects of selection and scaling procedures of earthquake records on the seismic response dispersion of structures and recommendations toward seismic upgrading of codes. Asian Journal of Civil Engineering. 2023 Jun 21:1-6. [View at Google Scholar]; [View at Publisher].

[53] Jiang W, Ling X, Yuan D, Xiao J, Ren X, Li J, Fu Z. Mechanical response of asphalt steel plastic pavement structure based on finite element simulation and scale load test. Construction and Building Materials. 2023 Dec 1;407:133490. [View at Google Scholar]; [View at Publisher].

[54] Sogabe T, Maki N. Do disasters provide an opportunity for regional development and change the societal trend of impacted communities?: Case study on the 1995 Kobe earthquake. International Journal of Disaster Risk Reduction. 2022 Jan 1;67:102648. [View at Google Scholar]; [View at Publisher].

[55] Mahdavi M. The world's great earthquakes the world's great earthquakes. LAP Lambert Academic Publishing; 2020.

[56] Su L, Ahmadi G. Probabilistic responses of base-isolated structures to El Centro 1940 and Mexico City 1985 earthquakes. Engineering Structures. 1992 Jan 1;14(4):217-30. [View at Google Scholar]; [View at Publisher].

[57] Takada S, Imanishi T. Time and Space Restoration Process and Prediction of Recovery Period for Damaged Water Supply Systems Based on GIS Data of The 1995 Kobe Earthquake. InAdvancing Mitigation Technologies and Disaster Response for Lifeline Systems 2003 (pp. 39-48). [View at Google Scholar]; [View at Publisher].

[58] Burkacki D, Jankowski R. Experimental Study on Steel Tank Model Using Shaking Table/Badania Eksperymentalne Modelu Zbiornika Stalowego Na Stole Sejsmicznym. Civil and environmental engineering reports. 2015 Feb 6;14(3):37-47. [View at Google Scholar]; [View at Publisher].

[59] Kazaz İ, Bilge İH, Gürbüz M. Near-fault ground motion characteristics and its effects on a collapsed reinforced concrete structure in Hatay during the February 6, 2023 Mw7. 8 Kahramanmaraş earthquake. Engineering Structures. 2024 Jan 1;298:117067. [View at Google Scholar]; [View at Publisher].

[60] Van Cao V. External GFRP confinement to decrease near-fault earthquake damage of reinforced concrete structures considering soil-structure interaction. InStructures 2021 Dec 1 (Vol. 34, pp. 2318-2339). Elsevier. [View at Google Scholar]; [View at Publisher].

[61] Ye L, Wang Y, Xie W. Seismic fragility and loss assessment on earthquake-resilient double-column tall piers with shear links subjected to far-field and near-fault ground motions. InStructures 2022 Nov 1 (Vol. 45, pp. 1774-1787). Elsevier. [View at Google Scholar]; [View at Publisher].

[62] Panahi FT, Morshedi AA, Talaeitaba SB. Effects of the structural dimensions of multi-span historical arched masonry buildings under near-fault and far-fault ground motions. Engineering Failure Analysis. 2023 Dec 1;154:107685. [View at Google Scholar]; [View at Publisher].

[63] Bilgin H, Hysenlliu M. Comparison of near and far-fault ground motion effects on low and mid-rise masonry buildings. Journal of Building Engineering. 2020 Jul 1;30:101248. [View at Google Scholar]; [View at Publisher].

[64]Abdollahzadeh D, Gerami M, Mastali M. Comparison Of Linear And Nonlinear Dynamic Methods Of Fema356 For Steel Moment Frames In Near And Far Field Of Faults. 2013. [View at Google Scholar]; [View at Publisher].

[65] Simpson G. Emergence and growth of faults during earthquakes: Insights from a dynamic elasto-plastic continuum model. Tectonophysics. 2023 Dec 5;868:230089. [View at Google Scholar]; [View at Publisher].

[66] Sadeghpour M, Kalatjari VR, Pahlavan H. Numerical study of the effect of geometric arrangement of the truss on the response modification factor of the special truss moment frame (STMF). SN Applied Sciences. 2021 May;3(5):584. [View at Google Scholar]; [View at Publisher].

[67] Mehta V, Chey MH. Seismic performance and assessment of RC framed structure with geometric irregularities. Asian Journal of Civil Engineering. 2023 Feb;24(2):479-96. [View at Google Scholar]; [View at Publisher].